Optical photon transport in powdered-phosphor scintillators. Part 1. Multiple-scattering and validity of the Boltzmann transport equation.

Gavin G. Poludniowski

Joint Department of Physics, Division of Radiotherapy and Imaging, Institute of Cancer Research and Royal Marsden NHS Foundation Trust, Downs Road, Sutton, Surrey, SM2 5PT, UK

Philip M. Evans

Centre for Vision Speech and Signal Processing (CVSSP), Faculty of Engineering and Physical Sciences, University of Surrey, Guildford, Surrey, GU2 7XH

ABSTRACT

Purpose: In Part 1 of this two-part work, predictions for light transport in powdered-phosphor screens are made, based on three distinct approaches. Predictions of geometrical optics-based ray tracing through an explicit microscopic model (EMM) for screen structure are compared to a Monte Carlo program based on the Boltzmann transport equation (BTE) and Swank's diffusion equation solution. The purpose is to: (I) highlight the additional assumptions of both the BTE Monte Carlo method and Swank's model (previously used in the literature) with respect to the EMM approach; (II) demonstrate the equivalences of the approaches under well-defined conditions and; (III) identify the onset and severity of any discrepancies between the models.

Methods: The EMM geometrical optics ray-tracing model is implemented for hypothesized micro-structures of phosphor grains in a binder. The BTE model is implemented as a Monte Carlo program with transport parameters, derived from geometrical optics, as inputs. The analytical solution of Swank to the diffusion equation is compared to the EMM and BTE predictions. Absorbed fractions and MTFs are calculated for a range of binder-to-phosphor relative refractive indices (n = 1.1 to 5.0), screen thicknesses (t = 50 to 200 μm) and packing fill factors (p_f = 0.04 to 0.54).

Results: Disagreement between BTE and EMM approaches increased with increasing n and p_f. For the thinnest screen (t = 50 μm), highest packing fill (p_f = 0.5) and largest relative refractive index (n = 5), the BTE model underestimated the absorbed fraction by 40% and the MTF50 by 20%. However, the BTE and EMM predictions agreed well at all simulated packing densities when $n \leq 2$. Swank's model agreed with the BTE well when the screen was thick enough to be considered turbid.

Conclusion: Although assumptions of the BTE are violated in powdered-phosphor screens at moderate-to-high packing densities, these lead to negligible effects in the modeling of optical transport for typical phosphor-binder relative refractive indices ($n \leq 2$), such as those based on Gd_2O_2S:Tb. Swank's diffusion equation solution is an adequate approximation to the BTE if the turbidity condition is satisfied.

I. INTRODUCTION

Many medical x-ray imaging systems use the indirect-detection of x-rays by fluorescing materials. An important class of such technologies uses powdered-phosphor screens, in which grains of a phosphor material are embedded within an inert binder material.[1] Powder-phosphor screens have been utilized in Computed Radiography,[2] Digital Radiography flat-panel detectors[3] and in Image-Guided Radiotherapy.[4] In such a detector, the spatial-resolution of the system is limited not only by x-ray and secondary electron interaction processes in the screen, but also by the spread of the generated optical photons prior to their detection at a photo-sensor. Light spread leads to degradation in the system modulation-transform-function (MTF) and light-collection-efficiency. This is the topic for this set of two publications in which the validity of modeling approaches and approximations is assessed. Interest in these effects of light spread and loss has been extensive.[5-17]

An optical photon emitted in a screen is expected to scatter many times from numerous grains of phosphor before detection. The regime of interest is typically where the emission wavelengths are in the visible region (λ < 1 μm) and are smaller than the grain radius (a > 1 μm). It might therefore be expected that geometrical optics provides a reasonable approximation[18] in the form of optical ray-

tracing, such as that implemented in the DETECT2000[19] and Geant4[20] Monte Carlo packages. Ray-tracing through an explicit screen microstructure is, however, a computationally approach. An attractive alternative is to treat a phosphor screen as an effective homogenous medium with associated scattering and absorption lengths. There is a long history of similar theoretical reductions[18] and the Boltzmann transport equation[6,9,12-16] (BTE) or diffusion equation[5,7,17] may be used to treat the multiple-scattering problem. The use of the BTE in a medium sparsely filled with scattering objects is well-motivated. The validity of its use in a more densely-packed medium is less clear[21] and particularly relevant because of the typical packing factors in real screens[13] and some researchers modeling of very high packing factors.[13-16] In Part 1 of this, predictions of an explicit microscopic model (EMM) based on geometrical optics are compared to those of both the BTE and a model derived from Swank's well-known diffusion equation solution.[5] A relatively abstract approach is taken: no attempt is made to model a particular real phosphor screen, but rather a range of ideal examples. This allows a particular theoretical question, the validity of a BTE approach, to be isolated in the simplest possible terms. The question of the accuracy of calculations of the transport cross-sections used is largely set aside here, geometrical optics being assumed valid. That assumption is, however, investigated in Part 2[22] in comparison to the more sophisticated approach of Mie-type theory.[18] The effects of x-ray dose-deposition, grain-size distribution and emission spectrum are also examined in Part 2 for examples of real screens, leading to comparison with other authors' experimental measurements.

II. METHOD AND MATERIALS

II.A Idealized powdered-phosphor screens

Grain size (or diameter) in phosphor screens are typically in the range 2 to 10 μm, with the smaller end of the range being preferred for high-resolution applications and larger for high speed screens.[23,24] In this study all the phosphor grains are considered to be spheres of identical radius, a = 3.5 μm, corresponding to an average phosphor powder size that is commercially available.[25] Note that this is also the median grain size in some general-purpose commercial screens.[23] The optical emission

wavelength in this study is set to, λ = 0.5 μm, which is approximately the peak emission for the Gd_2O_2S:Tb phosphor[13] used in Lanex screens.

The phosphor grains are embedded in a binder to form a slab-shaped screen. The complex refractive index (RI) of the grains is defined,

$$m_g = n_g - iz_g, \qquad (1)$$

where the imaginary component z_g describes the absorption strength of the phosphor material. Following previous authors, $z_g = 10^{-6}$ is used here.[13-16] The RI of the binder is assumed real and taken to be, n_b = 1.353 (appropriate to a Na_2SiO_3 binder[13]). The binder is assumed to neither scatter nor absorbs optical photons (although introducing an imaginary component would be appropriate for binders doped with absorptive dyes). The relative RIs of grain-to-binder will be used extensively and are defined as,

$$n = \frac{n_g}{n_b}; \text{ and } z = \frac{z_g}{n_b}. \qquad (2)$$

A broad range of n are examined (1.0 to 5.0) which more than encompasses the values typical for powder phosphors.[13-16] Zero reflectivity is assumed at the screen boundaries i.e. all optical photons reaching the front or back surface are transmitted. Simple extensions to the models could include non-zero reflectivity at these surfaces due to mismatches in the RI of the binder and the adjoining materials or the presence of reflective coatings.

For the purpose of this study a narrow pencil beam of incident x-rays is assumed to deposit energy in the phosphor along its path only and uniformly with depth. This avoids the necessity of modeling specific x-ray energies, x-ray attenuation coefficients, secondary electron propagation and K-edge x-ray fluorescence, all of which might have to be considered for any specific real screen,[13] but are irrelevant to the question of optical transport itself.

II.B Explicit microscopic model (EMM)

The EMM for optical transport assumes that a microscopic structure has been created consisting of N spherical grains of identical size packed into the screen. The fraction of screen volume filled with phosphor is the packing fill fraction and denoted p_f. Consider the path of a ray in a screen. Let $\boldsymbol{r}$ be the starting position and $\boldsymbol{r}'$ the finishing position. The path of a ray in the screen can be written as,

$$\boldsymbol{r}' = \boldsymbol{r} + s\boldsymbol{\Omega}, \quad (3)$$

where s is the path-length and $\boldsymbol{\Omega}$ is the direction-cosine vector. Fig. 1(a) depicts an intersection of a ray with a sphere and defines some relevant angles (θ, τ, θ', τ'). If $\boldsymbol{r}'$ is a point on the surface of the jth grain then equation for the sphere is,

$$\left|\boldsymbol{r}' - \boldsymbol{r}_j\right|^2 = a^2 \quad (4)$$

where the grain is centered at $\boldsymbol{r}_j$ and is of radius a. Solving (3) and (4) simultaneously, if any solution exists, yields the path-lengths at which the ray intersects the sphere. The smallest real positive solution for the set of N spheres yields the closest point of intersection. At such a point the ray may be transmitted (refracted) or reflected. The normal vector of the sphere surface at an intersection can be expressed as,

$$\boldsymbol{n} = \pm\frac{\boldsymbol{r}' - \boldsymbol{r}_j}{a}, \quad (5)$$

where the plus sign is taken if the ray intersects the sphere from outside the sphere and the minus if from the inside. The incident angle, θ, between the ray and sphere is then,

$$\cos\theta = -\boldsymbol{n}\cdot\boldsymbol{\Omega} = \sin\tau. \quad (6)$$

The real RI of the medium in which the incident ray is travelling is designated as n_1 (n_b or n_g) and the medium on the other side of the interface to be n_2 (n_g or n_b). If the outgoing direction of the ray is $\boldsymbol{\Omega}'$, then in the case of specular reflection,

$$\boldsymbol{\Omega}'_{\text{refl}} = \boldsymbol{\Omega} + 2\cos\theta\,\boldsymbol{n}. \quad (7)$$

In the case of refraction, from Snell's law,

$$\boldsymbol{\Omega}'_{tran} = \frac{n_1}{n_2}\Omega + \left(\frac{n_1}{n_2}\cos\theta - \sqrt{1-\sin^2\theta'}\right)\boldsymbol{n} \qquad (8)$$

where $n_2 \sin\theta' = n_1 \sin\theta$.[26] It remains to find the probability of reflection, R. If $n_1 > n_2$ then

$$R = 1 \text{ if } \theta \geq \sin^{-1}\frac{n_2}{n_1}, \qquad (9)$$

125 due to total internal reflection. Otherwise, the reflectance is given by the Fresnel coefficients,[18]

$$R = p_1 r_1^2 + (1-p_1) r_2^2 \quad (10)$$

where

$$r_1 = \frac{n_1\cos\theta - n_2\cos\theta'}{n_1\cos\theta + n_2\cos\theta'} = \frac{\sin(\tau-\tau')}{\sin(\tau+\tau')}, \qquad (11)$$

$$r_2 = \frac{n_2\cos\theta - n_1\cos\theta'}{n_2\cos\theta + n_1\cos\theta'} = \frac{\tan(\tau-\tau')}{\tan(\tau+\tau')}. \qquad (12)$$

130 The p_1 parameter is the degree to which the electric-field of the incident photon is polarized perpendicular to the plane defined by the incident and outgoing photon. The fate of a particular photon (transmission or reflection) can be found by random sampling. A photon is assumed unpolarized upon initial emission (p_1 = 0.5) but upon reflection/refraction it will not necessarily remain so. From Bayes' theorem, the probability that a photon is perpendicularly polarized (i.e. state

135 1) given that it is transmitted or across a boundary is,

$$p(1 \mid \text{tran}) = \frac{(1-r_1^2)p_1}{1-R}. \qquad (13)$$

The probability, given that it is reflected, is

$$p(1\,|\,\mathrm{refl}) = \frac{r_2^2 p_1}{R}. \qquad (14)$$

In either case, this probability is the new value for p_1 for the outgoing photon. Note that subsequent reflections and refractions within a sphere occur in the same plane and so transformations of polarization vectors are unnecessary: (13) or (14) can be applied repeatedly. However, on exiting the sphere, the photon state is again set as unpolarized. This partial treatment appears somewhat contrived but corresponds exactly to the typical Monte Carlo models for optical photon transport based on a scalar BTE (no polarization). The input transport cross-sections for such scalar BTE Monte Carlo models typically are derived including polarization states. Note that absorption may only occur within the phosphor grains and has the absorption coefficient,[18]

$$\mu_{abs} = 4\pi \frac{z_g}{\lambda}, \qquad (15)$$

where λ is the photon wavelength *in vacuo*.

The model described above can be implemented as follows. An emission point and initial direction of a photon are assigned using random sampling. A search is then conducted to find the nearest intersection by iterating through the N grains in the screen and solving (3) and (4). The photon is then transported to the intersection and reflection and transmission angles calculated using (5-8) and reflection/transmission determined based on (9-12), again, by random sampling. The photon is transported to successive interfaces by the same method until it escapes the screen. If the photon escapes the upper face of the screen it is assumed detected at the exit point. The survival probability of a photon transported a step of length s inside a grain is,

$$p(surv) = \exp(-s\mu_{abs}) \qquad (16)$$

and determined using (15) and random sampling once more.

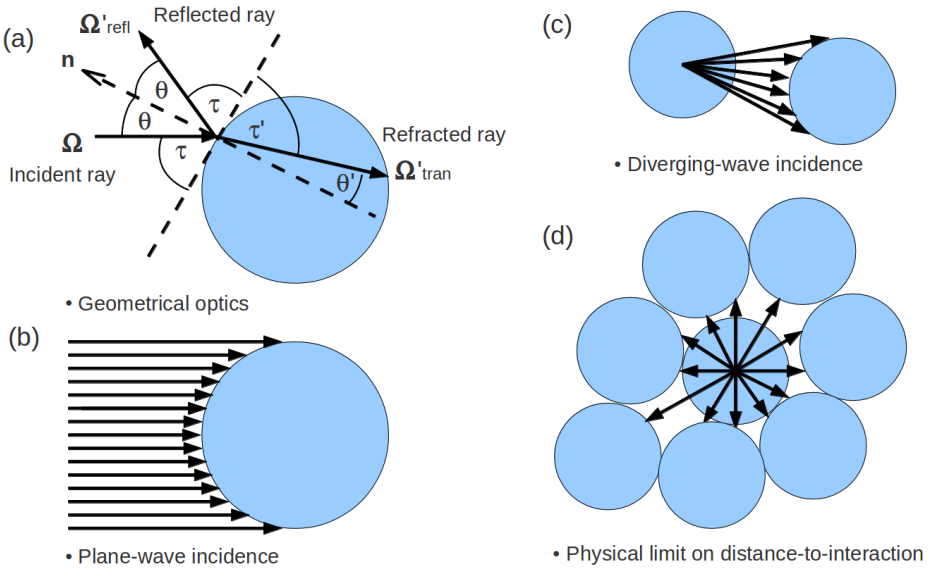

FIG. 1. Illustrations of: (a) the angles relating to the reflection or refraction of an incident ray from a sphere in geometrical optics, (b) plane-wave incidence on a sphere as a sum of multiple rays, (c) diverging-wave incidence on a sphere as a sum of multiple rays and (d) the physical limitation on distance-to-interaction with closely packed spheres.

II.C Scattering from a single sphere

In the previous subsection the transport of a photon through a large number of scattering spheres was discussed. Now, instead, a large number of photons corresponding to a wave-front, interacting with a single sphere will be considered. This is illustrated in Fig. 1(b) where the parallel incident rays correspond to an incoming plane-wave. The probability of interaction is related to the extinction efficiency factor, Q_{ext}. This is the sum of absorption (*abs*) and scatter (*sct*) components. In the geometrical optics model (GOM), all the energy falling on the particle is absorbed or reflected/refracted (scattered). This provides the result,

$$Q_{ext}^{GOM} = Q_{sct}^{GOM} + Q_{abs}^{GOM} = 1. \qquad (17)$$

The absorption efficiency can be calculated directly by summation of all orders of reflection and refraction. For weakly absorbing spheres, it takes the form[27]

$$Q_{abs}^{GOM} = \frac{16\pi}{3}\frac{an_b}{\lambda}\, z\, n^2\left(1-\left(1-n^{-2}\right)^{3/2}\right). \qquad (18)$$

It is likely that surface roughness and irregularities in a grain shape would modify equation (18) to some degree in a real phosphor screen, but given the uncertainties in *z* it may be sufficiently accurate approximately spherical grains. The scattering efficiency can then be found by the subtraction of (18) from (17), although $Q_{abs} << Q_{sct}$ and therefore $Q_{ext} \approx Q_{sct}$. The anisotropy factor, *g*, a measure of the degree of concentration of scatter in the forward direction, is defined as

$$g = \overline{\Omega\cdot\Omega'} = \frac{1}{Q_{sct}}\int_{-1}^{1}\Omega\cdot\Omega'\frac{dQ_{sct}}{d(\Omega\cdot\Omega')}d(\Omega\cdot\Omega'), \quad (19)$$

where $\boldsymbol{\Omega}\cdot\boldsymbol{\Omega}'$ is the cosine of the scattering angle. The form of the anisotropy factor, g^{GOM}, is also known:[18]

$$g^{GOM} = \frac{1}{2}\sum_{i=1,2}\int_0^1 \frac{2r_i^4(1-\cos 2\tau')\cos 2\tau + \left(1-r_i^2\right)^2\cos(2\tau-2\tau')}{1-2r_i^2\cos 2\tau' + r_i^4}d\left(\cos^2\tau\right) \qquad (20)$$

where r_1 and r_2 are the Fresnel reflection coefficients. Here scatter anisotropy depends only on relative RI: $g^{GOM}(n\to 1)=1$ and $g^{GOM}(n\to\infty)=0$. Note that a simple empirical approximation to (20) is proposed in Part 2. Again it is probable that surface roughness and departures from spherical grain form would quantitatively affect the anisotropy factor in a real screen.

The above transport parameters, Q_{abs}, Q_{sct} and *g* relate to transport in the bulk medium. If fraction of the volume filled with phosphor grains, p_f, is small, such that the grains are sparsely and randomly distributed, then the probability of interaction follows Poisson statistics. That is, the survival probability for a path-length step of *s* (without scatter or absorption) is,

$$p(\text{surv}) = \exp\left(-s\frac{p_f A}{V}\left(Q_{sct}+Q_{abs}\right)\right) = \exp\left(-\frac{s}{l_{ext}}\right), \qquad (21)$$

where l_{ext} is the extinction length and *V* and *A* are the volume and area of a grain, respectively.

II.D Boltzmann transport equation model

The photon flux ($m^{-2}s^{-1}sr^{-1}$) at a position $\boldsymbol{r}$ in a screen in the direction $\boldsymbol{\Omega}$ and at a time t can be denoted $\Phi(\boldsymbol{r},\boldsymbol{\Omega},t)$. The BTE for light transport, which describes the balance of five terms, is then,[28]

$$\underbrace{\left(\frac{1}{c}\frac{\partial}{\partial t}\right)}_{\text{I}}+\underbrace{\boldsymbol{\Omega}\cdot\nabla}_{\text{II}}+\underbrace{l_{ext}^{-1}}_{\text{III}}\Phi(\boldsymbol{r},\boldsymbol{\Omega},t)=\underbrace{l_{sct}^{-1}\int_{4\pi}d\Omega'\Phi(\boldsymbol{r},\boldsymbol{\Omega}',t)P(\boldsymbol{\Omega}\cdot\boldsymbol{\Omega}')}_{\text{IV}}+\underbrace{S(\boldsymbol{r},\boldsymbol{\Omega},t)}_{\text{V}}, \qquad (22)$$

where $P(\boldsymbol{\Omega}\cdot\boldsymbol{\Omega}')$ is the probability density for a photon to scatter to a direction $\boldsymbol{\Omega}$ from $\boldsymbol{\Omega}'$ and c is the speed of light in the medium. Terms I and II describe the leakage of photons out from a point $\boldsymbol{r}$ in a direction $\boldsymbol{\Omega}$ due to photon propagation. Term III describes the loss of photons at $\boldsymbol{r}$ and travelling in direction $\boldsymbol{\Omega}$ due to interactions at that point. Term IV describes the gain in photons at $\boldsymbol{r}$ travelling in direction $\boldsymbol{\Omega}$ due to scattering at that point from a direction $\boldsymbol{\Omega}'$. The final part, term V, describes the gain in photons at $\boldsymbol{r}$ due to a source, $S(\boldsymbol{r},\boldsymbol{\Omega},t)$, at that point. The photon current density, $\boldsymbol{j}(\boldsymbol{r},t)$, is defined

$$\boldsymbol{j}(\boldsymbol{r},t)=\int_{4\pi}d\Omega\,\boldsymbol{\Omega}\Phi(\boldsymbol{r},\boldsymbol{\Omega},t). \qquad (23)$$

If $\boldsymbol{r}'$ is a point on the detector surface and $\boldsymbol{n}$ the unit vector normal to the surface, then $\boldsymbol{j}(\boldsymbol{r},'t)\cdot\boldsymbol{n}$ is the number of photons detected per unit area per unit time. The forbidding-looking set of integro-differential equation (22-23) can be solved using Monte Carlo methods, in which photons are created and their histories simulated by sampling from the appropriate probability distribution functions. The boundary conditions are set by specifying a source term and imposing rules for any reflection at the boundaries. We refer the reader to prior work concerning the implementation of such a Monte Carlo.[13]

Most rigorously, a full theoretical expression for the scattering distribution, $P(\boldsymbol{\Omega}\cdot\boldsymbol{\Omega}')$, should be used. However, one of two approximations is often made. An empirical parameterization of the

scattering distribution can be chosen that satisfies an arbitrary value of anisotropy, $g = \overline{\boldsymbol{\Omega} \cdot \boldsymbol{\Omega}'}$, such as the Henyey-Greenstein distribution:[13]

$$P_{HGA}(\boldsymbol{\Omega} \cdot \boldsymbol{\Omega}') = \frac{1}{4\pi} \frac{1-g^2}{\left(1+g^2-2g\,\boldsymbol{\Omega} \cdot \boldsymbol{\Omega}'\right)^{3/2}} \qquad (24)$$

Alternatively, in the diffusion approximation, a reduced scattering length, $l_{sct}^* = l_{sct}/(1-g)$, can be defined and isotropic scattering assumed.[29] Then, l_{ext}^*, is the total reduced extinction length where. $l_{ext}^{*\,-1} = l_{abs}^{-1} + l_{sct}^{*\,-1}$. In either case only three independent transport parameters need be calculated: Q_{abs}, Q_{sct} and g.

Two of the assumptions of the BTE are, however, that:[21]

1. Interaction locations are far apart so that a scattered wave-front approximates a plane-wave.
2. The probability distribution functions for interactions follow Poisson statistics.

The EMM approach described in subsection II.B assumes neither of these points and in this respect it is more general. Fig. 1(c) and 1(d) illustrates how the two assumptions above fail for dense packing of grains. In Fig. 1(c) the emission point is located close to a second grain and the wave-front diverges, thus not well-approximating the plane-wave illustrated in Fig. 1(b). In Fig. 1(d) the proximity of surrounding phosphor grains on all sides limits the maximum distance an emitted photon can propagate before interacting: clearly the distance-to-interaction cannot follow Poisson statistics. However, the important question is: does the failure of the above assumptions matter? With a large number of collisions and a randomly arranged set of phosphor grains, do the effects average out? These questions have not previously been addressed in the literature.

II.E Diffusion equation and Swank's solution

A first order approximation to the BTE is the diffusion equation, which may be written:

$$\left(\frac{1}{c}\frac{\partial}{\partial t}-\frac{1}{3}l_{ext}^{*}\nabla^{2}\right)\phi(\boldsymbol{r})+l_{abs}^{-1}\phi(\boldsymbol{r})=s(\boldsymbol{r}), \quad (25)$$

where,

$$\phi(\boldsymbol{r},t)=\int_{4\pi}\Phi(\boldsymbol{r},\boldsymbol{\Omega},t)d\Omega \text{ and } s(\boldsymbol{r},t)=\int_{4\pi}S(\boldsymbol{r},\boldsymbol{\Omega},t)d\Omega. \quad (26)$$

The reader is referred to Ref. 28 for a clear derivation of the diffusion equation from (22). Swank has demonstrated how to solve the steady-state form of (25) in slab geometry to obtain the MTF and the detected fraction (η_{det}) of optical photons. The precise form of Swank's solution for the idealized screens and line emission-source modeled in this work is derived in Appendix A. Swank's solution, which has been widely used as the basis of models,[15,17,30] is included for comparison with the predictions of the EMM and BTE approaches. Note that one of the assumptions of the diffusion equation (but not of the BTE or EMM) is that the screen thickness is such that, $t >> l_{sct}^{*}$. This is the definition of a "turbid" medium. It can be concluded that Swank's diffusion model will be likely to be applicable when,

$$t >> t_c \equiv l_{sct}^{*}\big|_{sphere}=\frac{4a}{3p_f}\frac{1}{1-g^{GOM}}, \quad (27)$$

where t_c is the critical screen thickness. When this condition is not satisfied a screen is optically "thin".

II.F Computational methods and implementation

The transport parameters proposed in II.C were used as inputs into the BTE and Swank models. The EMM and BTE Monte Carlo programs described in II.B and II.D were coded in Fortran 95 and compiled with the Intel Fortran Compiler V12. A computer cluster was used for calculations with nodes consisting of two six-core 3.4 GHz CPUs, with 8 GB RAM per CPU. BTE and EMM simulations were run with 24 threads using the OpenMP library of the Intel compiler and hyperthreading. The number of optical histories simulated, *H*, was set to:

$$H = \frac{Q}{p_f t}, \qquad (28)$$

where t is the screen thickness and Q was set to $2\text{x}10^6$ and $100\text{x}10^6$, for EMM and BTE simulations, respectively. The use of equation (28) ensured approximately uniform uncertainties in the absorbed fractions of photons (≈ 10% and ≈ 2%, for EMM and BTE simulations, respectively). Simulations consisted of 18 sets for each method (6 n values and 3 t values) with each set consisting of 11 values of p_f. Each of the 18 sets of simulations took 1 to 16 hours (EMM) and 2 to 6 hours (BTE) depending on particular (n, t) combination.

Some remarks are necessary about the realization of a microscopic structure for EMM simulations of screens. It should be noted that arbitrarily high packing fill factors cannot be obtained due to the lack of tessellation of spheres: there are always void spaces that must be filled by binder. The Kepler conjecture states that a packing fill factor higher than that of a regular face-centered-cubic (FCC) arrangement cannot be obtained for equal-sized spheres. That packing fill factor is, $p_f^{FCC} \approx 0.74$.[31] Irregular-packing of equal spheres are limited to packing factors substantially less than the FCC maximum. A random packing algorithm was written that was capable of realizing packing factors, for equally sized spheres, of up to a maximum: $p_f^{rand} = 0.54$. This is typical of the packing fill factors in powdered-phosphor screens.[32] Packing factors lower than the limit were realized by scaling the sphere separations.

The optical photon emission source within the screen was chosen as a line-source for the BTE (see Section II.A), in which the screen is considered a homogenous medium. In the EMM, however, photon emission could only occur from where such a line intersected a phosphor grain. Every photon history in the simulation therefore used a new microstructure of grains to produce overall an average line-source. In the EMM model, for some combinations of source-locations within a grain and direction of emission, a photon is trapped by total internal reflection. Such photons were rejected. The absorbed fraction, η_{abs}, should therefore be interpreted as the fraction of photons that escape the grain in which they are emitted and then are absorbed prior to detection.

The pre-sampled MTF was calculated from the simulated histories as follows (see Appendix B for derivation):

$$MTF(w) = \frac{1}{D}\sum_{i=1}^{D} J_0(2\pi\rho_i w), \quad (29)$$

where D is the number of detected photons, $\rho_i = \left(x_i^2 + y_i^2\right)^{1/2}$ is its lateral displacement and w is the spatial frequency (cycles/mm).

The predictions for Swank's model were calculated using equations (A3-A5) of Appendix A.

III. RESULTS

Presented in Fig. 2(a) to 2(f) are the predictions for η_{abs} in the three models (EMM, BTE, Swank), against p_f, for six values of relative RIs. The associated statistical uncertainties are appreciable only for the EMM model. Agreement between the EMM and BTE is good, for $n \leq 2$, but deteriorates at higher relative RI. Discrepancies in absorption are most apparent between the EMM and BTE in the thickest screen (t = 200 μm,) combined with the highest relative RI (n = 5). Swank's diffusion model generally agrees well with the BTE, although there are indications of increasing discrepancy with reducing relative RI. This is expected, due to the increased scatter anisotropy with reduced value of n.

Presented in Fig. 3(a) to 3(f) are the MTF50 predictions, again varying with p_f, for the six relative RIs and the three models. The associated statistical uncertainties are smaller than the marker size in all cases and not shown. Again, agreement between the EMM and BTE model predictions are good, for $n \leq 2$. Discrepancies become apparent for higher relative RIs and are worse for thinner screen thickness. The agreement of Swank's model to the BTE is poor for the MTF50 statistic where the turbidity condition (27) is not satisfied (where $p_f \rightarrow 0$, $n \rightarrow 1$).

A more complete picture of the lateral spread of photons is given by the full MTFs. These are presented for the BTE and EMM in Fig. 4(a) to 4(f) for the highest simulated packing densities for each simulated n and t. The agreement in BTE and EMM curves is good except for $n > 2$, as expected

from the MTF50 statistic. Fig. 5(a) to 5(f) compare the BTE and Swank's model predictions for the MTFs. The agreement of Swank's model with the BTE is excellent where the screen is not "thin".

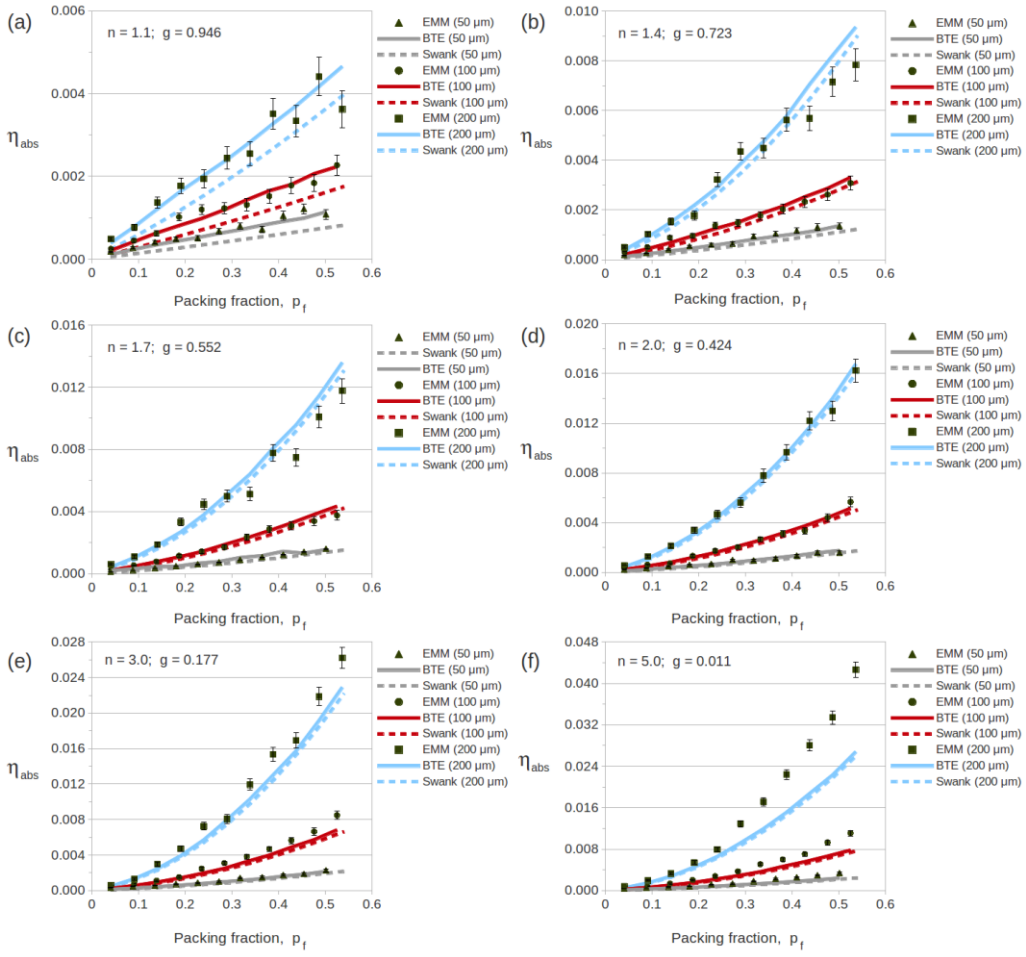

310 FIG. 2. Absorption fraction, η_{abs}, for three thicknesses of screen (t = 50, 100 and 200 μm) and six relative RIs: (a) 1.1, (b) 1.4, (c) 1.7, (d) 2.0, (e) 3.0 and (f) 5.0. Results shown as a function of packing fill factor, p_f. Solid and broken lines are predictions of the BTE and Swank's model, respectively and data points those of the EMM. Relative RIs (n) and anisotropy factors (g) are shown.

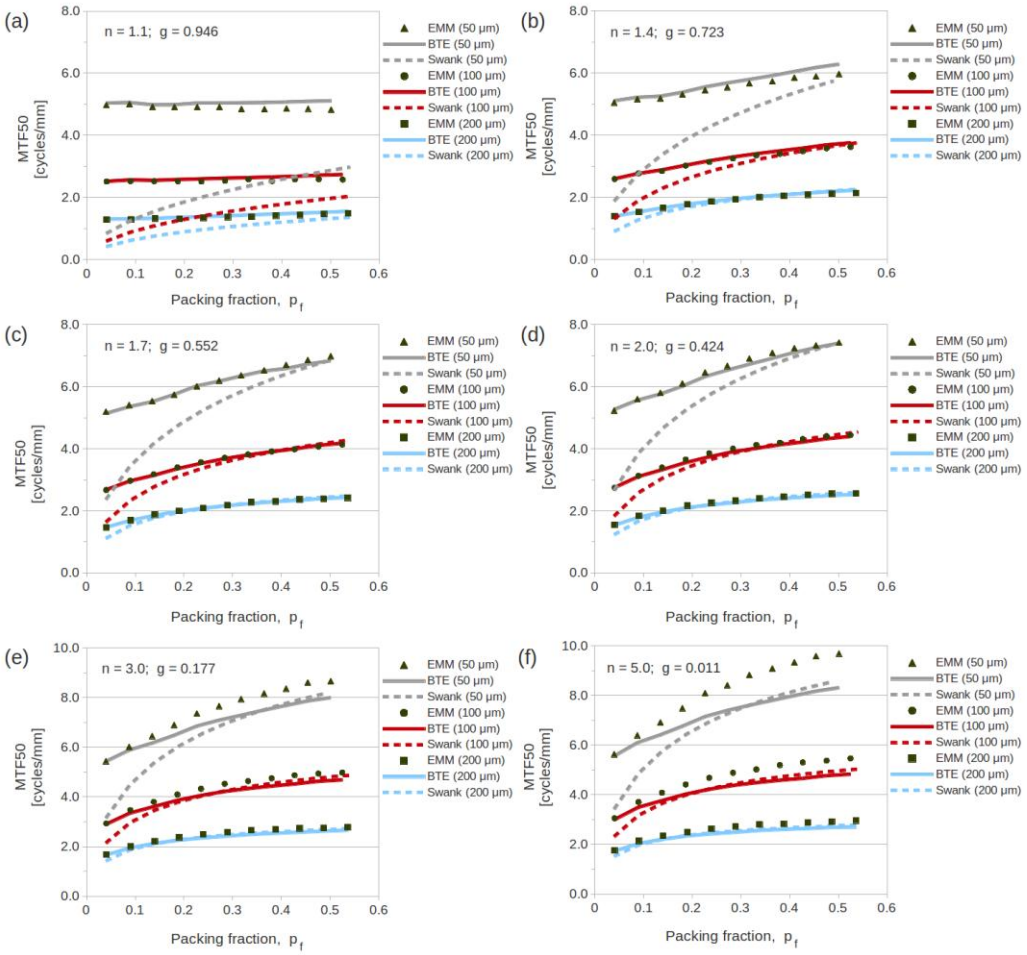

315

FIG. 3. MTF50 for three thicknesses of screen (t = 50, 100 and 200 µm) and six relative RIs: (a) 1.1, (b) 1.4, (c) 1.7, (d) 2.0, (e) 3.0 and (f) 5.0. Results shown as a function of packing fill factor, p_f. Solid and broken lines are predictions of the BTE and Swank's model, respectively and data points those of the EMM. Relative RIs (n) and anisotropy factors (g) are shown.

320

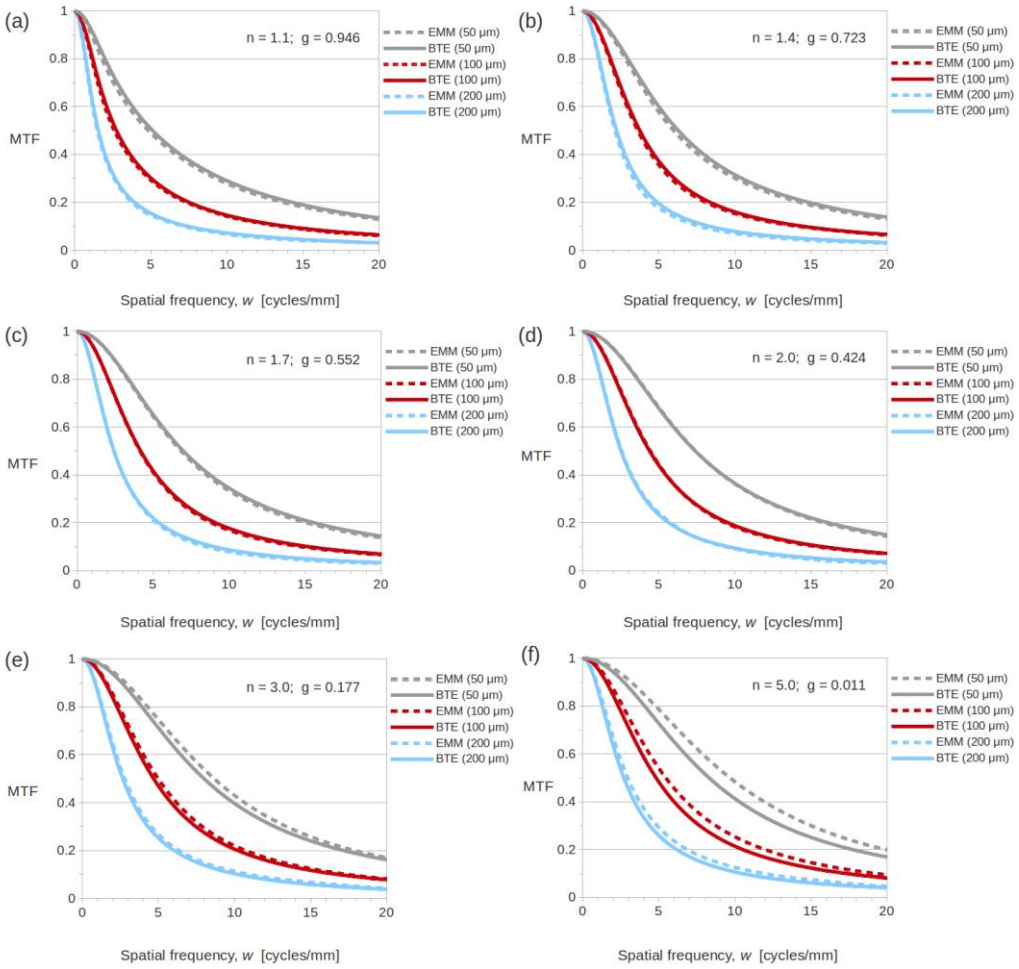

FIG. 4. MTFs for three thicknesses of screen (t = 50, 100 and 200 µm) and six relative RIs: (a) 1.1, (b) 1.4, (c) 1.7, (d) 2.0, (e) 3.0 and (f) 5.0. Results shown are for maximum realized fill factors ($p_f \approx 0.5$). Solid lines are predictions of the BTE and dashed lines those of the EMM. Relative RIs (n) and anisotropy factors (g) are shown.

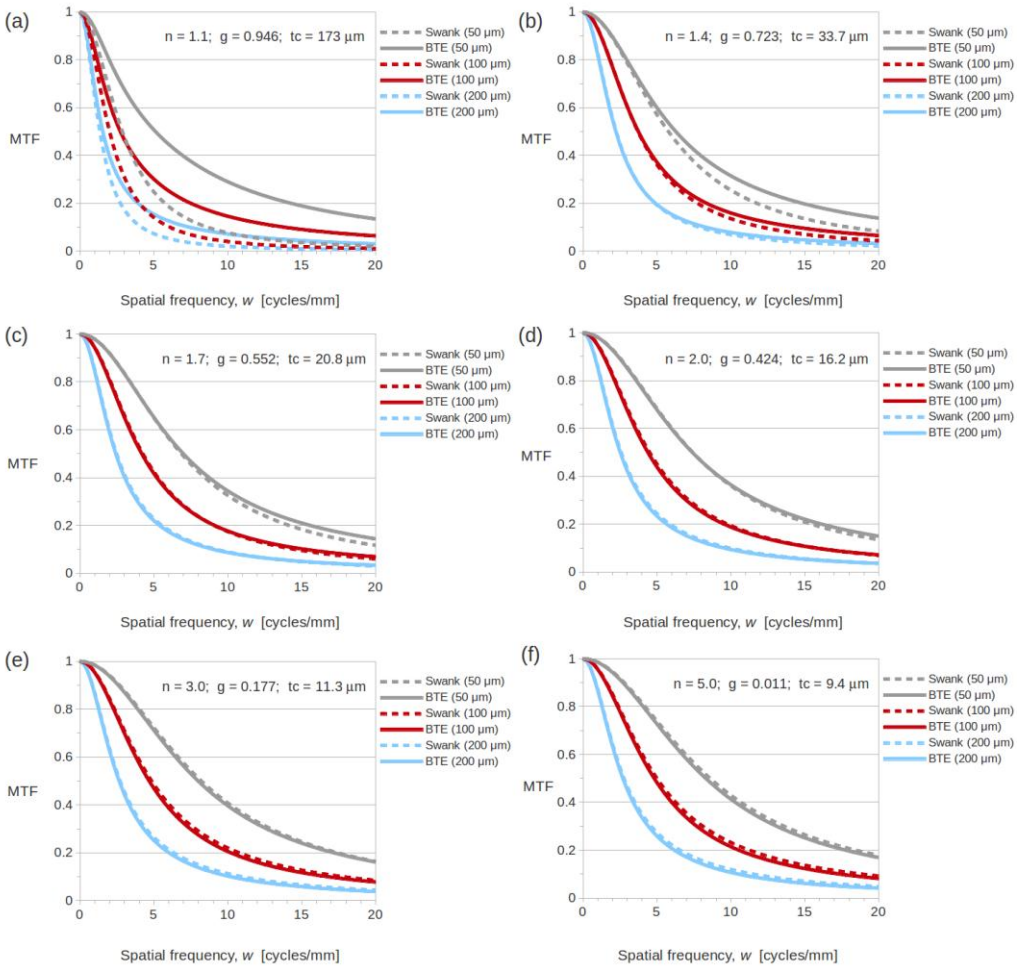

330 FIG. 5. MTFs for three thicknesses of screen (t = 50, 100 and 200 µm) and six relative RIs: (a) 1.1, (b) 1.4, (c) 1.7, (d) 2.0, (e) 3.0 and (f) 5.0. Results shown are for maximum realized fill factors ($p_f \approx 0.5$). Solid lines are predictions of the BTE and dashed lines those of the Swank's model. Relative RIs (n), anisotropy factors (g) and critical thicknesses (t_c) are shown.

335 **IV. DISCUSSION**

In subsection II.D it was argued that the Boltzmann transport equation relies on assumptions that are not strictly satisfied for powdered-phosphor screens with high packing densities. What is of practical importance is whether this leads to substantial errors for phosphor screens of plausible composition and geometry. In this study an explicit microscopic model of reflection and refraction, which does not

340 make the plane-wave and Poisson interaction assumptions of the BTE, was used to validate against

the BTE and Swank's well-known diffusion model. On the whole it might be said that the BTE does better than one has a right to expect, even for the cases of densely-packed phosphor grains. The results presented demonstrate that the EMM and BTE model predictions correspond well for all examined screen thicknesses (50-200 μm), when $n \leq 2.0$. This range of RIs covers that of all commonly used phosphor materials. The BTE is therefore recommended over the EMM approach because of their relative efficiencies. In our implementations, the BTE Monte Carlo was approximately 50x faster on average. This was mainly due to the inefficiency of an exhaustive search through all spheres conducted in the EMM at each step, to find the closest point of intersection for a photon. As expected, Swank's model based on the diffusion equation agreed well with the BTE, except for non-turbid or "thin" screens ($t << t_c$). Swank's solution has the advantage of an analytic form, although such an analytic expression is only possible for simple absorbed energy distributions such as an exponential or line-source, the latter of which was considered here.

Of course, the nature of energy–deposition in a phosphor due to x-ray and secondary electron transport and matters like boundary reflectivity must be considered in any thorough treatment of powdered-phosphor screens that aims to compare to experiment. Beyond these issues, however, the idealized screens modeled in this study resemble real screens, in many respects such as packing density, relative RI and emission wavelength (see Section II.A). Note however that a real phosphor does emit a spectrum of wavelengths around a peak wavelength (or multiple peaks). Further there are large deviations from a spherical shape for many phosphor materials and always a distribution in grains size. More fundamentally, geometrical optics, assumed to be valid here, is itself an approximation. Geometrical optics has allowed a direct comparison between equivalent EMM, BTE and Swank models, however, it is only an approximation to Maxwell's equations and hence the scattering problem. Most of these issues are explored further in Part 2.

V. CONCLUSION

The apparent consequences of the breakdown of assumptions of the Boltzmann transport equation (BTE) are slight for typical phosphor materials and RIs. Comparison with an explicit microscopic

model of transport has shown that Monte Carlo and predictions based on the BTE should provide reasonable predictions of MTF and absorbed fraction. Swank's diffusion model also agrees well with the BTE, when a screen can be considered turbid.

VI. APPENDIX

A. Swank's solution

Swank derived the optical transfer function for photons emitted in a turbid medium and slab geometry, within the approximation of the diffusion equation. For an optical emission at depth *z*, in a screen of thickness *t* with zero reflectivity at the boundaries, the function is:

$$G(w;z)=3\frac{\left(2l_{ext}^{*}q+3\right)e^{qz}+\left(2l_{ext}^{*}q-3\right)e^{-qz}}{\left(2l_{ext}^{*}q+3\right)^{2}e^{qt}-\left(2l_{ext}^{*}q-3\right)^{2}e^{-qt}} \quad \text{(A1)}$$

where

$$q=\left(4\pi^{2}w^{2}+\sigma^{2}\right)^{1/2} \quad \text{and} \quad \sigma=\sqrt{3/l_{ext}^{*}l_{abs}}\,. \quad \text{(A2)}$$

For a screen with line source emission, the detected fraction, η_{det}, is:

$$\eta_{\det}=\frac{1}{t}\int_{o}^{t}G(0;z)dz=\frac{6}{\sigma t}\frac{2l_{ext}^{*}\sigma\sinh\sigma t+3(\cosh\sigma t-1)}{\left(2l_{ext}^{*}\sigma+3\right)^{2}e^{\sigma t}-\left(2l_{ext}^{*}\sigma-3\right)^{2}e^{-\sigma t}}, \quad \text{(A3)}$$

and for the special case of the idealized screen considered here (line-source and zero reflectivity),

$$\eta_{abs}=1-2\eta_{\det} \quad \text{(A4)}$$

The presampled MTF is then:

$$\begin{aligned}MTF(w)&=\frac{1}{\eta_{\det}}\frac{1}{t}\int_{o}^{t}G(w;z)dz\\&=\left[\frac{2l_{ext}^{*}q\sinh qt+3(\cosh qt-1)}{2l_{ext}^{*}q\sinh\sigma t+3(\cosh\sigma t-1)}\right]\left[\frac{\left(2l_{ext}^{*}\sigma+3\right)^{2}e^{\sigma t}-\left(2l_{ext}^{*}\sigma-3\right)^{2}e^{-\sigma t}}{\left(2l_{ext}^{*}q+3\right)^{2}e^{qt}-\left(2l_{ext}^{*}q-3\right)^{2}e^{-qt}}\right].\end{aligned} \quad \text{(A5)}$$

B. Presampled MTF

It is assumed that the Point-Spread-Function (PSF) of a screen has circular symmetry. The 2D Fourier transform of the PSF (the MTF) then reduces to a Hankel transform:

$$MTF(w) = \int \exp(2\pi i\, \boldsymbol{\rho} \cdot \boldsymbol{w}) PSF(\boldsymbol{\rho}) d^2\rho$$
$$= \int_0^\infty \int_0^{2\pi} \exp(2\pi i\, \rho w \cos\theta) PSF(\rho) d\theta \rho d\rho = 2\pi \int_0^\infty J_0(2\pi\rho w) PSF(\rho) \rho d\rho \quad \text{(B1)}$$

The Monte Carlo results for the distribution of lateral displacements of photons at the detector can be used to conduct a Monte Carlo integration of the above Hankel transform yielding,

$$MTF(w) = 2\pi \int_0^\infty J_0(2\pi\rho w) PSF(\rho) \rho d\rho = \lim_{D\to\infty} \frac{1}{D} \sum_{i=1}^{D} J_0(2\pi\rho_i w). \quad \text{(B2)}$$

If D is large enough the summation provides an accurate presampled MTF. The MTF is presampled in the sense that it has not derived from data in which photons have been binned into pixels.

ACKNOWLEDGEMENTS

This work was partially supported by research Grant No. C46/A10588 from Cancer Research UK.

The authors acknowledge NIHR funding to the NHS Biomedical Research Center.

REFERENCES

[1]M. Nikl, "Scintillation detectors for x-rays," Meas. Sci. Technol. 17, R37–R54 (2006).

[2]J. A. Rowlands, "The physics of computed radiography" Phys. Med. Biol. 47, R123–R166 (2002).

[3]J. A. Seibert, "Flat-panel detectors: how much better are they?" Pediatr Radiol. 36 S2, 173-81 (2006).

[4]M. C. Kirby, A. G. Glendinning, "Developments in electronic portal imaging systems," Br J Radiol. 79 S1:S50-65 (2006).

[5]R. K. Swank, "Calculation of modulation transfer functions of x-ray fluorescent screens," Applied optics 12(8), 1865-1870 (1973).

[6]R. Morlotti, "X-ray efficiency and modulation transfer function of fluorescent Rare Earth screens, determined by the Monte Carlo method," J. Photographic Sci. 23, 181-189 (1975).

[7]J. A. Seibert, O. Nalcioglu, and W. W. Roeck, "Characterization of the veiling glare PSF in x-ray image intensified fluoroscopy," Med. Phys. 11(2), 172-179 (1984).

[8]G. E. Giakoumakis, M. C. Katsarioti, I. E. Lagaris, and G. S. Panayiotakis, "A theoretical model for the x-ray luminescence of granular phosphor screens," J. Appl. Phys. 69, 6607-6610 (1991).

[9]T. Radcliffe, G. Barnea, B. Wowk, R. Rajapakshe, S. Shalev, "Monte Carlo optimization of metal/phosphor screens at megavoltage energies," Med Phys. 20(4), 1161-9 (1993).

[10]J. Lindström and G. A. Carlsson, "A simple model for estimating the particle size dependence of absolute efficiency of fluorescent screens," Phys Med Biol. 44(5), 1353-67 (1999).

[11]C. Kirkby and R. Sloboda, "Comprehensive Monte Carlo calculation of the point spread function for a commercial a-Si EPID," Med Phys. 32(4), 1115-27 (2005).

[12]S. Pistrui-maximean, N. Freud, J. Letang, A. Koch, B. Munier, A. Walenta, G. Montarou, D. Babot, "Geant4 simulation of the response of phosphor screens for X-ray imaging," Nuclear Instruments and Methods in Physics Research A563(1), 196-199 (2006).

[13]P. F. Liaparinos, I. S. Kandarakis, D. A. Cavouras, H. B. Delis, G. S. Panayiotakis, "Modeling granular phosphor screens by Monte Carlo methods," Med Phys. 33(12), 4502-14 (2006).

[14]P. F. Liaparinos, I. S. Kandarakis, D. A. Cavouras, H. B. Delis, G. S. Panayiotakis, "Monte Carlo study on the imaging performance of powder Lu2SiO5:Ce phosphor screens under x-ray excitation: comparison with Gd2O2S:Tb screens," Med Phys. 34(5), 1724-33 (2007).

[15]P. F. Liaparinos, I. S. Kandarakis, "The Monte Carlo evaluation of noise and resolution properties of granular phosphor screens," Phys Med Biol. 54(4), 859-74 (2009).

[16]P. F. Liaparinos, I. S. Kandarakis, "The imaging performance of compact Lu2O3:Eu powdered phosphor screens: Monte Carlo simulation for applications in mammography," Med Phys. 36(6), 1985-97 (2009).

[17]R. J. Acciavatti and A. D. Maidment, "Optimization of phosphor-based detector design for oblique x-ray incidence in digital breast tomosynthesis," Med Phys. 38(11), 6188-6202 (2011).

[18]H. C. van de Hulst, *Light Scattering by Small Particles* (Dover, New York, 1981).

[19]F. Cayouette, D. Laurendeau and C. Moisan, "DETECT2000: an improved Monte-Carlo simulator for the computer aided design of photon sensing devices," Proc. SPIE 4833, 69 (2003).

[20]S. Agostinelli et al, "Geant4 – a simulation toolkit," Nucl. Instrum. and Methods in Phys. Res. A 506, 250-303 (2003).

[21]A. Lagendijk and B.A. van Tiggelen, "Resonant Multiple Scattering of Light," Physics Reports 270, 143-215 (1996).

[22]G. G. Poludniowski and P. M. Evans, "Optical photon transport in powdered-phosphor scintillators. Part 2. Calculating single-scattering transport parameters," submitted to Med. Phys. (2012).

[23]R. E. Dickerson and P. C. Bunch, "Minimal crossover radiographic elements adapted for varied intensifying screen exposures," US Patent No. 5108881 (1992).

[24]R. E. Dickerson, K. A. Duke and A. S. Fitterman, "Reflective radiographic material with incorporated developer," US Patent No. 7014977 (2006).

[25]I. Kandarakis and D. cavouras, "Experimental and theoretical assessment of the performance of Gd2O2S:Tb and La2O2S:Tb phosphors and Gd2O2S:Tb-La2O2S:Tb mixtures for x-ray imaging," Eur. Radiol. 11, 1083-1091 (2001).

[26]J. Albrecht, R. Seidel, L. Melzer, and D. Muller, "System-level optical models of 3-D laser projection systems using micromirror arrays," 2nd International Conference on Modeling and Simulation of Microsystems, 679-682 (1999).

[27]S. Twomey and C. F. Bohren, "Simple approximations for calculations of absorption in clouds," J. Atmos. Science 37(9), 2086-2094 (1980).

[28] R. C. Haskell, L. O. Svaasand, T-T Tsay, T-C Feng, M. S. McAdams, and B. J. Tromberg, "Boundary conditions for the diffusion equation in radiative transfer," JOSA A 11(10), 2727-2741 (1994).

[29]V. Tuchin, *Tissue optics: light scattering methods and instruments for medical diagnosis* (SPIE Press, 2007).

[30]N. Kalivas, L. Costaridou, I. Kandarakis, D. Cavouras, C. D. Nomicos and G. Panayiotakis, "Modelling quantum and structure noise of phosphors used in medical x-ray imaging detectors," Nucl. Instrum. Methods. Phys. Res. A 490, 614-629 (2002).

[31]T. C. Hales, "A proof of the Kepler conjecture," Annals of mathematics 162(3), 1063-1185 (2005).

[32]M. K. Cho, H. K. Kim, T. Graeve, S. M. Yun, C. H lim, H Cho and J-M Kim, "Measurements of x-ray imaging performance of granular phosphors with direct-coupled CMOS sensors," IEEE Trans. On Nucl. Sci. 55(3), 1338-1343 (2008).